

# Fluctuation-induced Néel and Bloch skyrmions at topological insulator surfaces

Flavio S. Nogueira,<sup>1,2</sup> Ilya Eremin,<sup>2,3</sup> Ferhat Katmis,<sup>4,5</sup> Jagadeesh S. Moodera,<sup>4,6</sup> Jeroen van den Brink,<sup>1,7</sup> and Volodymyr P. Kravchuk<sup>1,8</sup>

<sup>1</sup>*Institute for Theoretical Solid State Physics, IFW Dresden, Helmholtzstr. 20, 01069 Dresden, Germany*

<sup>2</sup>*Institut für Theoretische Physik III, Ruhr-Universität Bochum, Universitätsstraße 150, DE-44801 Bochum, Germany*

<sup>3</sup>*National University of Science and Technology MISiS, Moscow, 119049, Russia*

<sup>4</sup>*Francis Bitter Magnet Lab and Plasma Science and Fusion Center, Massachusetts Institute of Technology, Cambridge, MA 02139, USA*

<sup>5</sup>*Department of Physics, Middle East Technical University, 06800 Ankara, Turkey*

<sup>6</sup>*Department of Physics, Massachusetts Institute of Technology, Cambridge, MA-02139, USA*

<sup>7</sup>*Institute for Theoretical Physics, TU Dresden, 01069 Dresden, Germany*

<sup>8</sup>*Bogolyubov Institute for Theoretical Physics of National Academy of Sciences of Ukraine, 03680 Kyiv, Ukraine*

(Dated: Received August 7, 2018)

Ferromagnets in contact with a topological insulator have become appealing candidates for spintronics due to the presence of Dirac surface states with spin-momentum locking. Because of this bilayer  $\text{Bi}_2\text{Se}_3$ -EuS structures, for instance, show a finite magnetization at the interface at temperatures well exceeding the Curie temperature of bulk EuS. Here we determine theoretically the effective magnetic interactions at a topological insulator-ferromagnet interface *above* the magnetic ordering temperature. We show that by integrating out the Dirac fermion fluctuations an effective Dzyaloshinskii-Moriya interaction and magnetic charging interaction emerge. As a result individual magnetic skyrmions and extended skyrmion lattices can form at interfaces of ferromagnets and topological insulators, the first indications of which have been very recently observed experimentally.

PACS numbers: 75.70.-i, 73.43.Nq, 64.70.Tg, 75.30.Gw

*Introduction*— The spin-momentum locking property of three-dimensional topological insulators (TIs) [1, 2] make them promising candidate materials for future spin-based electronic devices. One important consequence of spin-momentum locking in TIs is the topological electromagnetic response, which arises from induced Chern-Simons (CS) terms [3] on each surface [4]. This happens for instance when time-reversal (TR) symmetry is broken, which renders the surface Dirac fermions gapped. This can be achieved, for example, by proximity-effect with a ferromagnetic insulator (FMI) [5–15]. In this case, a CS term is generated if there are an odd number of *gapped* Dirac fermions, which is achieved only in the presence of out-of-plane exchange fields [11]. The realization of several physical effects related to the CS term that have been predicted in the literature critically depend on growing technologies required for the fabrication of heterostructures involving both strong TIs and FMIs. Recently, high quality  $\text{Bi}_2\text{Se}_3$ -EuS bilayer structures have been shown to exhibit proximity-induced ferromagnetism on the surface of  $\text{Bi}_2\text{Se}_3$  [6, 16, 17]. Other successful realizations of the stable ferromagnetic TI interfaces were demonstrated recently [18, 19]. In addition it was shown that the interface of FMI and TI can have magnetic ordering temperature much higher than the bulk ordering temperature [5], indicating that topological surface states can strongly affect the magnetic properties of a proximity-coupled FMI.

These experimental advances motivate us to investigate the effective magnetic interactions that result from

the fluctuating momentum-locked Dirac fermion surface states of a TI in contact with an FMI. We show that even in the absence of any spontaneous magnetization, at temperatures above the Curie temperature of the FMI, intriguing topologically stable magnetic textures, i.e., skyrmions, are induced as a result of quantum fluctuations of the Dirac fermions at the interface. In fact, we demonstrate that integrating out Dirac fermions coupled to a FMI thin film generates a Dzyaloshinskii-Moriya interaction (DMI), that depending on the form of the Dirac Hamiltonian, favors either Néel- or Bloch-type skyrmions [20–23]. However, skyrmions induced in TI-FMI structures feature in addition a “charging energy”, due to the generation of a term proportional to the square of the so called magnetic charge,  $\nabla \cdot \mathbf{n}$ , where  $\mathbf{n}$  denotes the direction of the magnetization [24]. An important feature of our finding is that the Dirac fermions that are integrated out *are not gapped*, since there is no spontaneous magnetization above  $T_c$  that would lead to a gap in the Dirac spectrum. Furthermore, the generated DMI is only nonzero if the chemical potential does not vanish. We obtain the phase diagram for the skyrmion solutions and identify the region of stability for skyrmion lattices in presence of the magnetic charging energy. This region we determine numerically by analyzing the excitation spectrum of the skyrmion solution. An important discovery is that the magnetic charging energy modifies the phase diagram significantly in the case of DMIs favoring Néel skyrmions, the situation relevant for  $\text{Bi}_2\text{Se}_3$ -EuS interface. Our theoretical findings support conceptually the

recent experimental observation of a skyrmion texture at a ferromagnetic heterostructure of Cr doped  $\text{Sb}_2\text{Te}_3$  [19]. Having a skyrmion profile on a TI surface will cause significant changes in the conductance that may be observed in transport measurements [25].

*Interface exchange interactions*— The Hamiltonian governing the Dirac fermions at the interface of a FMI/TI heterostructure has the general form,

$$H_{\text{Dirac}}(\mathbf{n}(\mathbf{r})) = [\mathbf{d}(-i\hbar\nabla) - J_0\mathbf{n}(\mathbf{r})] \cdot \boldsymbol{\sigma}, \quad (1)$$

where  $\mathbf{r} = (x, y)$ ,  $\boldsymbol{\sigma} = (\sigma_x, \sigma_y, \sigma_z)$  is a vector of Pauli matrices and  $J_0$  is the interface exchange coupling. The operator  $\mathbf{d}$  is a function of the momentum operator  $-i\hbar\nabla$ . Here we consider the two possibilities leading to a Dirac spectrum,

$$\mathbf{d}_1 = -i\hbar v_F \nabla, \quad \mathbf{d}_2 = -i\hbar v_F \nabla \times \hat{\mathbf{z}}, \quad (2)$$

with the latter arising in TIs like  $\text{Bi}_2\text{Se}_3$ ,  $\text{Bi}_2\text{Te}_3$ , and  $\text{Sb}_2\text{Te}_3$  [26]. Experimentally, in order for the effective Hamiltonian (1) to give a valid low-energy description of the physics at the interface, the TI must be at least 7 nm thick. The end result will be that  $\mathbf{d}_1$  induces a DMI of the type  $\mathbf{n} \cdot (\nabla \times \mathbf{n})$ , which is often referred to as a bulk DMI, but for clarity we call it *Bloch DMI*. Instead  $\mathbf{d}_2$  leads to different type of DMI,  $\sim \mathbf{n} \cdot [(\hat{\mathbf{z}} \times \nabla) \times \mathbf{n}] = (\mathbf{n} \cdot \nabla)n_z - n_z(\nabla \cdot \mathbf{n})$ , in the magnetic literature sometimes known as surface DMI, but to which we refer as *Néel DMI*.

The effective energy  $E_{\text{eff}}$  of the system is obtained by integrating out the Dirac fermions  $c = (c_\uparrow, c_\downarrow)$  in the partition function,

$$e^{-\beta E_{\text{eff}}(\mathbf{n})} = e^{-\beta \rho_s L \int_S dS (\nabla \mathbf{n})^2} \times \int \mathcal{D}c^\dagger \mathcal{D}c e^{-\int_0^\beta d\tau \int d^2r c^\dagger [\partial_\tau - \mu + H_{\text{Dirac}}(\mathbf{n}(\mathbf{r}))] c}, \quad (3)$$

where  $\rho_s$  is the magnetization stiffness of the FMI,  $L$  is the film thickness and the integration is over the film area  $S$ . Due to the nonzero  $z$ -component of the magnetization, the above model yields a gapped Dirac spectrum for  $T < T_c$  with spin wave excitations, which give rise to a Chern-Simons term [10]. However, this gap does not occur for  $T > T_c$ . In the following we assume that the gap vanishes for  $T \geq T_c$  and obtain the corresponding corrections to the free energy after integrating out the gapless Dirac fermions.

*Effective free energy and induced DMI*— The non-interacting Green function for a spin-momentum locked system can be written in general as

$$\mathcal{G}_{\alpha\beta}(\omega_n, \mathbf{k}) = G(\omega_n, \mathbf{k}) \delta_{\alpha\beta} + \mathbf{F}(\omega_n, \mathbf{k}) \cdot \boldsymbol{\sigma}_{\alpha\beta}, \quad (4)$$

where  $\omega_n = (2n+1)\pi/\beta$  is the fermionic Matsubara frequency. From the Hamiltonian (1) and the functional integral in (3) we have,

$$G(\omega_n, \mathbf{k}) = \frac{i\omega_n + \mu}{(i\omega_n + \mu)^2 - \mathbf{d}^2(\mathbf{k})}, \quad (5)$$

$$\mathbf{F}(\omega_n, \mathbf{k}) = -\frac{\mathbf{d}(\mathbf{k})}{(i\omega_n + \mu)^2 - \mathbf{d}^2(\mathbf{k})}, \quad (6)$$

where  $\mathbf{d}(\mathbf{k})$  is either  $\mathbf{d}_1$  or  $\mathbf{d}_2$  from Eq. (2) in momentum space. Integrating out the fermions and expanding the free energy expression up to  $J_0^2$ , we obtain after a long but straightforward calculation, the following correction to the effective free energy density [27]

$$\delta\mathcal{F}_{\text{Dirac}}^{\text{mag}} = \frac{s}{2} \{ [\nabla \mathbf{n}(\mathbf{r})]^2 + [\nabla \cdot \mathbf{n}(\mathbf{r})]^2 \} + i\frac{a}{2} \mathbf{n}(\mathbf{r}) \cdot [\mathbf{d}(-i\hbar\nabla) \times \mathbf{n}(\mathbf{r})], \quad (7)$$

where  $(\nabla \mathbf{n})^2 = \sum_{i=x,y,z} (\nabla n_i)^2$  defines the usual exchange term, and we have defined  $s = \beta J_0^2 / [24\pi \cosh^2(\beta\mu/2)]$  and  $a = J_0^2 (8\pi\hbar v_F)^{-1} \tanh(\beta\mu/2)$ . We can drop the constant term  $F_{\text{Dirac}}(0)$  from the free energy, since it does not depend on the field. Thus, we can safely write  $\mathcal{F}_{\text{Dirac}} = \delta\mathcal{F}_{\text{Dirac}}$ . The above expression features a DMI induced by Dirac fermion fluctuations. In addition, a contribution  $\sim (\nabla \cdot \mathbf{n})^2$  is also generated. We will see below that the presence of this term leads to interesting physical properties when  $\mathbf{d}_2$  is replaced for  $\mathbf{d}$  in Eq. (7), modifying in this way the behavior of Néel skyrmions. Note that differently from the case where the Dirac fermion is gapped [15], no intrinsic anisotropy is generated by the Dirac fermions. At the same time, we note that the form of  $\delta\mathcal{F}_{\text{Dirac}}^{\text{mag}}$  including the DMI term will persist also below  $T_c$  as long as the chemical potential is outside the gap, meaning that the TI surface is metallic, despite the generated mass  $m$  for the Dirac fermions.

*Effective magnetic energy in an external field*— The contributions from the FMI and Dirac fermions allows one to recast the effective energy for a thin ferromagnetic layer in the form,

$$E_{\text{eff}} = L \int_S \{ A [(\nabla \mathbf{n})^2 + \epsilon(\nabla \cdot \mathbf{n})^2] + D\mathcal{E}_{\text{DMI}} + M_s H(1 - n_z) \} dS, \quad (8)$$

where  $A = \rho_s + s/(2L)$  is the effective magnetization stiffness including the fluctuations due to the Dirac fermions. We assumed that the sample lies in the presence of an external magnetic field  $H$  applied perpendicular to it. We have also introduced the parameter  $\epsilon = s/(2AL) = s/(2\rho_s L + s)$ . The DM coupling is given by  $D = a/(2L)$ . The DM interaction has the possible forms,  $\mathcal{E}_{\text{DMI}}^{\text{B}} = \mathbf{n} \cdot (\nabla \times \mathbf{n})$  or  $\mathcal{E}_{\text{DMI}}^{\text{N}} = n_z \nabla \cdot \mathbf{n} - \mathbf{n} \cdot \nabla n_z$ , depending on whether  $\mathbf{d}_1$  or  $\mathbf{d}_2$  arises in the Dirac Hamiltonian (1). The latter is more adequate for  $\text{Bi}_2\text{Se}_3$ -EuS samples [13]. The ab initio results from Ref. 28 indicate that  $J_0$  is largely enhanced due to RKKY interactions at the  $\text{Bi}_2\text{Se}_3$ -EuS interface, ranging from 35 to 40 meV. Using  $J_0 = 35$  meV one can estimate that at room temperature  $s \in [0.05, 0.63]$  meV, and therefore  $\epsilon \in [0.08, 0.51]$

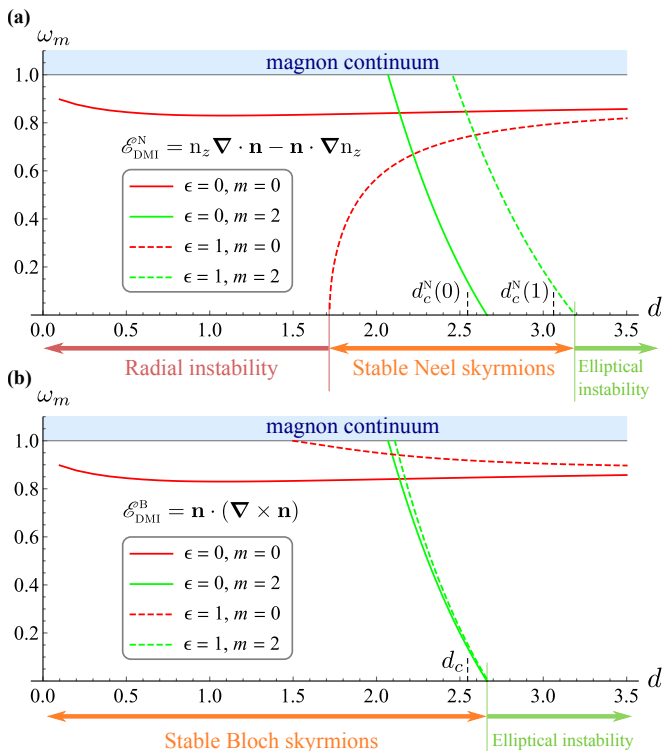


FIG. 1. Eigenfrequencies of two localized modes, namely radially-symmetric ( $m = 0$ ) and elliptic ( $m = 2$ ) are found by means of numerical solution of the eigenvalue problem for different DM terms. Modes, which do not demonstrate instability, are not shown. Stability/instability regions are indicated for the case  $\epsilon = 1$ .

for 1 nm thick film and  $\mu \in (0, 0.1]$  eV [29]. Note that  $\epsilon$  strongly depends on the value of  $\mu$ , which can be reduced by doping.

Although the temperature fluctuations usually destroys skyrmions in thin films, the individual skyrmions [30–32] as well as skyrmion lattices [33] are observed in various multilayer structures for room temperatures. Therefore, in experiments, it is reasonable to use a multilayer structure in form of the periodically repeated stack TI/FMI/NI, where NI is a normal insulator. In the following we neglect the influence of the thermal fluctuations on the magnetization structure, which holds when model (8) is applied for a multilayer structure.

Before studying the energy functional (8), let us emphasize that while the DMI is absent for the case of a vanishing chemical potential, the term  $(\nabla \cdot \mathbf{n})^2$  is always there, even if  $\mu = 0$ . Thus, this term is a unique feature of thin film FMIs proximate to a three-dimensional TI. In fact, it has been recently demonstrated that it is also induced for  $\mu = 0$  at zero temperature when the surface Dirac fermions are gapped by proximity effect to the FMI [15].

Ground states of system (8) are well studied for the case  $\epsilon = 0$  [34–38]. The uniform saturation along the

field is the ground state with  $E_{\text{eff}} = 0$  for large field and weak DM interaction, and 1D structure in form of periodical sequence of  $2\pi$  domain walls is the ground state with  $E_{\text{eff}} < 0$  for small fields and strong DM interaction. The criterion for the periodical state appearance is negative energy of a single domain wall, it reads  $d > d_c = 8/\pi$ , where  $d = \sqrt{2D}/\sqrt{AM_s H}$  is dimensionless DM constant. In vicinity of the boundary  $d \approx d_c$ , an intermediate phase in form of 2D periodical structure (skyrmion lattice) forms the ground state [20, 21, 34, 39]. An isolated skyrmion [21, 22, 35, 40] may appear as a topologically stable excitation of the uniformly saturated state. The skyrmions and domain walls are of Bloch and Néel types for the DM interaction in form  $\mathcal{E}_{\text{DMI}}^{\text{B}}$  and  $\mathcal{E}_{\text{DMI}}^{\text{N}}$ , respectively.

Here we study how the ground states and individual skyrmions are changed when  $\epsilon > 0$ . Since  $\nabla \cdot \mathbf{n} \equiv 0$  for any domain wall and skyrmion of the Bloch type (induced by  $\mathcal{E}_{\text{DMI}}^{\text{B}}$ ) the influence of the term  $(\nabla \cdot \mathbf{n})^2$  is not significant in this case. However, it drastically changes the ground state digram and stability of the static solutions for the case of  $\mathcal{E}_{\text{DMI}}^{\text{N}}$ . In this case,  $d_c = d_c^{\text{N}}(\epsilon) = (8/\pi) \int_0^1 \sqrt{1 + \epsilon(2\xi^2 - 1)^2} d\xi$  and period of the 1D structure is increased with  $\epsilon$  [27]. Energy per period is  $E_{\text{1D}}^{\text{N}}(d, \epsilon) \approx AL\mathcal{E}(d, \epsilon)$ , where  $\mathcal{E}(d, \epsilon)$  is determined by the implicit relation  $d/d_c^{\text{N}}(\epsilon) = E(4/\mathcal{E})/\sqrt{-\mathcal{E}/4}$ , with  $E(k)$  being the complete elliptic integral of the second kind [41] (note that  $\mathcal{E} < 0$ ). For the case  $\mathcal{E}_{\text{DMI}}^{\text{B}}$  the 1D periodical structure is not affected by  $\epsilon$  and one has  $d_c^{\text{B}} = d_c^{\text{N}}(0)$  and  $E_{\text{1D}}^{\text{B}}(d) = E_{\text{1D}}^{\text{N}}(d, 0)$  [27].

*Skyrmion solutions* —Here we consider the topologically stable excitations of the saturated state  $\mathbf{n} = \hat{z}$ . First, we utilize the constraint  $\mathbf{n}^2 = 1$  by expressing the direction of the magnetization in spherical coordinates,  $\mathbf{n} = \sin\theta(\cos\phi\hat{x} + \sin\phi\hat{y}) + \cos\theta\hat{z}$ . One can show [27] that for the case  $\mathcal{E}_{\text{DMI}}^{\text{N}}$  the total energy (8) has a local minimum if  $\phi = \chi$  and function  $\theta = \theta(\rho)$  is determined by the equation

$$(1 + \epsilon \cos^2 \theta) \nabla_{\rho}^2 \theta - \sin \theta \cos \theta \left( \frac{1 + \epsilon}{\rho^2} + \epsilon \theta'^2 \right) + d \frac{\sin^2 \theta}{\rho} - \sin \theta = 0, \quad (9)$$

where  $\rho$  we introduced the polar frame of reference  $\{\rho, \chi\}$  with the radial distance  $\rho$  measured in units of  $\ell = \sqrt{2A/(M_s H)}$  and  $\nabla_{\rho}^2 f = \rho^{-1} \partial_{\rho}(\rho \partial_{\rho} f)$  denotes radial part of the Laplace operator. Equation (9) must be solved with the boundary conditions  $\theta(0) = \pi$ ,  $\theta(\infty) = 0$ . A number of examples of skyrmion profiles determined by Eq. (9) for various values of parameters  $d$  and  $\epsilon$  are shown in Fig. S2 [27]. Note that the skyrmion size is mainly determined by the parameter  $d$ , while the parameter  $\epsilon$  weakly modifies the details of the skyrmion profile. For the case  $\mathcal{E}_{\text{DMI}}^{\text{B}}$  the equilibrium solution is  $\phi = \chi + \pi/2$  and the corresponding equation for the profile  $\theta(\rho)$  coincides

with (9) when  $\epsilon = 0$ . Note that in this case Eq. (9) is reduced to the well known skyrmion equation [23, 34, 40].

In order to analyze stability of the obtained static solutions we study spectrum of the skyrmion eigenexcitations by means of the methods commonly applied for skyrmions [38, 42] as well as for others two-dimensional magnetic topological solitons [43–47]. Namely, we introduce time-dependent small deviations  $\theta = \theta_0 + \vartheta$  and  $\phi = \phi_0 + \varphi/\sin\theta_0$ , where  $\vartheta, \varphi \ll 1$  and  $\theta_0 = \theta_0(\rho)$ ,  $\phi_0$  denotes the static profile. The linearization of the Landau-Lifshitz equations,  $\sin\theta\partial_t\phi = \frac{\gamma}{M_s}\delta E_{\text{eff}}/\delta\theta$ ,  $-\sin\theta\partial_t\theta = \frac{\gamma}{M_s}\delta E_{\text{eff}}/\delta\phi$ , in the vicinity of the static solution results in solutions for the deviations in the form  $\vartheta = f(\rho)\cos(\omega\tau + m\chi + \chi_0)$ ,  $\varphi = g(\rho)\sin(\omega\tau + m\chi + \chi_0)$ , where  $m \in \mathbb{Z}$  is an azimuthal quantum number and  $\chi_0$  is an arbitrary phase. Here  $\tau = t\Omega_0$  is the dimensionless time, where  $\Omega_0 = \gamma H$  is the Larmor frequency with  $\gamma$  being the gyromagnetic ratio. The eigenfrequencies  $\omega$  and the corresponding eigenfunctions  $f, g$  are determined by solving the Bogolyubov-de Gennes eigenvalue problem [27]. The numerical solution was obtained for a range of  $d$  and a couple of values of  $\epsilon$ . A number of bounded eigenmodes with  $\omega < 1$  are found in the gap. Eigenfrequencies of the radially-symmetric ( $m = 0$ ) and elliptic ( $m = 2$ ) modes are shown in Fig. 1, where we compare both types of DM terms [48]. If  $\epsilon = 0$ , the spectra are identical for both cases, in particular, the well known elliptical instability [35, 38] take place due to the softening of the elliptic mode in the region  $d > d_c$ , where the uniformly saturated state is thermodynamically unstable [38]. For the case  $\mathcal{E}_{\text{DMI}}^{\text{N}}$  the  $\epsilon$ -term shifts the elliptical instability to the larger values of  $d$  with the condition  $d > d_c^{\text{N}}(\epsilon)$  kept, while in the case  $\mathcal{E}_{\text{DMI}}^{\text{B}}$  the effect of the  $\epsilon$ -term is negligible.

Remarkably, the  $\epsilon$ -term influences oppositely on the breathing mode ( $m = 0$ ), for different DM types. For the case  $\mathcal{E}_{\text{DMI}}^{\text{B}}$  the eigenfrequency  $\omega_0$  is increased and for small  $d$  the breathing mode is pushed out from the gap into the magnon continuum. As a result, the small-radius skyrmions are free of the bounded states. This is in contrast to the case  $\mathcal{E}_{\text{DMI}}^{\text{N}}$ , when the breathing mode eigenfrequency is rapidly decreased resulting in a radial instability for small  $d$ . In order to give some physical insight to the latter effect we consider the model, where the skyrmion profile is described by the linear Ansatz [23, 34]  $\theta_a(\rho) = \frac{\pi}{R}(R - \rho)\text{H}(R - \rho)$ , and  $\phi = \chi + \Phi$ . Here the variational parameters  $R$  and  $\Phi$  describe the skyrmion radius and helicity, respectively, and  $\text{H}(x)$  is the Heaviside step function. For this model total energy (8) with  $\mathcal{E}_{\text{DMI}} = \mathcal{E}_{\text{DMI}}^{\text{N}}$  reads

$$\frac{E_{\text{tot}}^{\text{N}}}{2\pi AL} = e_{\text{ex}} + \epsilon e_{\epsilon} \cos^2\Phi - 2\delta \cos\Phi R + R^2 e_{\text{H}}, \quad (10)$$

where the constants  $e_{\text{ex}} \approx 6.15$  [49],  $e_{\epsilon} = e_{\text{ex}} - \pi^2/4$  and  $e_{\text{H}} = 1 - 4/\pi^2$  originate from the exchange,  $\epsilon$ -term and Zeeman contributions, respectively. Here  $\delta = d\pi/4$ . The

energy expression (10) shows that the equilibrium helicity  $\Phi$  is determined by the competition of the  $\epsilon$ -term, which tends to  $\Phi = \pm\pi/2$  (Bloch skyrmion), and the DM term, which tends to  $\Phi = 0$  (Néel skyrmion). In the same time, the equilibrium skyrmion radius is determined by the competition of the DM and Zeeman terms, and for the Bloch skyrmion one has  $R = 0$ . Thus, the skyrmion collapse is expected with the  $\epsilon$  increasing. Indeed, the minimization of the total energy (10) with respect to the both variational parameters results in the critical value  $\epsilon_c = \delta^2/(e_{\epsilon}e_{\text{H}})$ : if  $\epsilon < \epsilon_c$  then the equilibrium values of the variational parameters  $R_0 = \delta/e_{\text{H}}$  and  $\Phi_0 = 0$  determines the Néel skyrmion; if  $\epsilon > \epsilon_c$  that the minimum of energy (10) is reached for  $R_0 = 0$  and  $\Phi_0 = \pm\pi/2$ . The latter corresponds to a collapsed Bloch skyrmion. In other words, a stable Néel skyrmion exists for the case  $\epsilon < \epsilon_c$ . Surprisingly, there are no intermediate states with  $0 < \Phi_0 < \pi/2$  when  $\epsilon > \epsilon_c$ .

*Skyrmion lattice* — In order to estimate the region of existence of the skyrmion lattice we use the circular cell approximation [34], when the lattice cell is approximated by a circle of radius  $R$  and the boundary condition  $\theta(R) = 0$  is applied. The skyrmion profile is described by the same linear Ansatz as for the case of an isolated skyrmion. Minimizing the energy (10) per unit cell  $E_{2\text{D}}^{\text{N}} = E_{\text{tot}}^{\text{N}}/(\pi R^2)$  one obtains the following equilibrium values of the variational parameters  $\Phi_0^{\text{N}} = 0$ ,  $R_0^{\text{N}}(\epsilon) = (e_{\text{ex}} + \epsilon e_{\epsilon})/\delta$ , and the corresponding equilibrium energy reads  $E_{2\text{D}}^{\text{N}}(\epsilon) = 2AL [e_{\text{H}} - \delta^2/(e_{\text{ex}} + \epsilon e_{\epsilon})]$ . For the case  $\mathcal{E}_{\text{DMI}}^{\text{B}}$  the same procedure results in the  $\epsilon$ -independent values:  $\Phi_0^{\text{B}} = \pi/2$ ,  $R_0^{\text{B}} = R_0^{\text{N}}(0)$  and  $E_{2\text{D}}^{\text{B}} = E_{2\text{D}}^{\text{N}}(0)$ .

Comparing energies of three states, namely, the energy of the uniform magnetization along field  $E = 0$ , energy of the 1D periodical state (per period)  $E_{1\text{D}}$ , and energy of the skyrmion lattice per unit cell  $E_{2\text{D}}$ , we determine the phase diagram of the ground states, see Fig. 2. Note that for  $\epsilon > \epsilon_0 \approx 0.98$  the skyrmion lattice is not a ground state. Given the dependence of  $\epsilon$  with the exchange coupling  $J_0$ , temperature, and chemical potential, the skyrmion lattice phase is likely to occur for a not too high temperature range as compared to the Curie temperature of EuS. The dimensionless DM parameter  $d$  can then be tuned by the external field to attain the interval shown under the green area of Fig. 2(a).

*Conclusions* — We have shown that the effective magnetic energy for a TI-FMI heterostructure exhibits a Dzyaloshinskii-Moriya term induced by tracing out the surface Dirac fermions proximate to the FMI. A unique feature of the effective energy as compared to other DM systems is the presence of an additionally induced magnetic capacitance energy, given by a term proportional to the square of the magnetic charge  $\nabla \cdot \mathbf{n}$ . Despite having a small magnitude in realistic samples, the interplay between this term and the DM one yields a phase diagram with interesting phase boundaries in the case of a Néel DMI, which is the situation relevant for, e.g.,  $\text{Bi}_2\text{Se}_3$

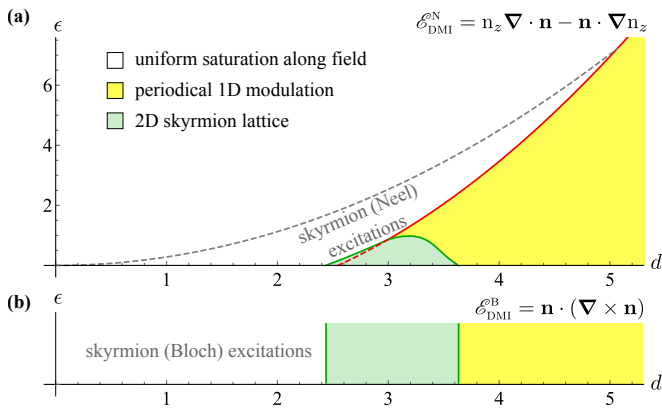


FIG. 2. Diagrams of the ground states for different kinds of DMI. (a): the red line is determined by the condition  $d = d_c^n(\epsilon)$ , it separates the uniform state and periodical 1D modulation. The green region of the Néel skyrmion lattices is determined by the conditions  $E_{2D}^N < E_{1D}^N$  and  $E_{2D}^N < 0$  to the right and to the left of the red line. The gray dashed line is the line of collapse of the Néel skyrmions, it is determined by the condition  $\epsilon = \epsilon_c(d)$ . (b): colors have the same meaning as on the panel (a), but periodical helical state and skyrmion lattices are of Bloch type. The excitations in form of isolated Bloch skyrmions are stable within all white region. If  $\mathbf{d}_1$  is used in the Hamiltonian (1), the coefficient of the  $(\nabla \cdot \mathbf{n})^2$  would be negative, which would in turn make the Bloch skyrmion more stable

samples proximate to a FMI. Our theory is directly relevant for very recently synthesized TI - ferromagnetic thin film heterostructures, in some of which the formation of a skyrmionic magnetic texture has been observed [19].

F.S.N. and I.E. thank the DFG Priority Program SPP 1666, "Topological Insulators", under Grant number, ER 463/9. J.v.d.B. acknowledges support from SFB 1143. FK and JSM. acknowledge the support from NSF Grants No. DMR-1207469, 1700137 ONR Grant No. N00014-13-1-0301, N00014-16-1-2657 and the STC Center for Integrated Quantum Materials under NSF Grant No. DMR-1231319. F.K. acknowledges the Science and Technological Research Council of Turkey (TUBITAK) through the BIDEB 2232 Program under award number 117C050 (Low-Dimensional Hybrid Topological Materials). I.E. acknowledges support by the Ministry of Education and Science of the Russian Federation in the framework of Increase Competitiveness Program of NUST MISiS (K2-2017-085).

- 
- [1] M. Z. Hasan and C. L. Kane, "Colloquium : Topological insulators," *Reviews of Modern Physics* **82**, 3045–3067 (2010).  
 [2] Xiao-Liang Qi and Shou-Cheng Zhang, "Topological insulators and superconductors," *Reviews of Modern Physics* **83**, 1057–1110 (2011).

- [3] S. Deser, R. Jackiw, and S. Templeton, "Three-dimensional massive gauge theories," *Physical Review Letters* **48**, 975–978 (1982); A. J. Niemi and G. W. Semenoff, "Axial-anomaly-induced fermion fractionization and effective gauge-theory actions in odd-dimensional space-times," *Physical Review Letters* **51**, 2077–2080 (1983); A. N. Redlich, "Parity violation and gauge non-invariance of the effective gauge field action in three dimensions," *Physical Review D* **29**, 2366–2374 (1984).  
 [4] Xiao-Liang Qi, Taylor L. Hughes, and Shou-Cheng Zhang, "Topological field theory of time-reversal invariant insulators," *Physical Review B* **78**, 195424 (2008).  
 [5] Ferhat Katmis, Valeria Lauter, Flavio S. Nogueira, Badih A. Assaf, Michelle E. Jamer, Peng Wei, Biswarup Satpati, John W. Freeland, Ilya Eremin, Don Heiman, Pablo Jarillo-Herrero, and Jagadeesh S. Moodera, "A high-temperature ferromagnetic topological insulating phase by proximity coupling," *Nature* **533**, 513–516 (2016).  
 [6] Peng Wei, Ferhat Katmis, Badih A. Assaf, Hadar Steinberg, Pablo Jarillo-Herrero, Donald Heiman, and Jagadeesh S. Moodera, "Exchange-coupling-induced symmetry breaking in topological insulators," *Physical Review Letters* **110**, 186807 (2013).  
 [7] Ion Garate and M. Franz, "Inverse spin-galvanic effect in the interface between a topological insulator and a ferromagnet," *Physical Review Letters* **104**, 146802 (2010).  
 [8] Takehito Yokoyama, Jiadong Zang, and Naoto Nagaosa, "Theoretical study of the dynamics of magnetization on the topological surface," *Physical Review B* **81**, 241410(R) (2010).  
 [9] Yaroslav Tserkovnyak and Daniel Loss, "Thin-film magnetization dynamics on the surface of a topological insulator," *Phys. Rev. Lett.* **108**, 187201 (2012).  
 [10] Flavio S. Nogueira and Ilya Eremin, "Fluctuation-induced magnetization dynamics and criticality at the interface of a topological insulator with a magnetically ordered layer," *Physical Review Letters* **109**, 237203 (2012).  
 [11] Flavio S. Nogueira and Ilya Eremin, "Semimetal-insulator transition on the surface of a topological insulator with in-plane magnetization," *Physical Review B* **88**, 085126 (2013).  
 [12] Yaroslav Tserkovnyak, D. A. Pesin, and Daniel Loss, "Spin and orbital magnetic response on the surface of a topological insulator," *Physical Review B* **91**, 041121(R) (2015).  
 [13] Mingda Li, Wenping Cui, Jin Yu, Zuyang Dai, Zhe Wang, Ferhat Katmis, Wanlin Guo, and Jagadeesh Moodera, "Magnetic proximity effect and interlayer exchange coupling of ferromagnetic/topological insulator/ferromagnetic trilayer," *Physical Review B* **91**, 014427 (2015).  
 [14] Stefan Rex, Flavio S. Nogueira, and Asle Sudbø, "Non-local topological magnetoelectric effect by coulomb interaction at a topological insulator-ferromagnet interface," *Physical Review B* **93**, 014404 (2016).  
 [15] Stefan Rex, Flavio S. Nogueira, and Asle Sudbø, "Topological magnetic dipolar interaction and nonlocal electric magnetization control in topological insulator heterostructures," *Physical Review B* **94**, 020404(R) (2016).  
 [16] Qi I. Yang, Merav Dolev, Li Zhang, Jinfeng Zhao, Alexander D. Fried, Elizabeth Schemm, Min Liu, Alexander Palevski, Ann F. Marshall, Subhash H. Risbud,

- and Aharon Kapitulnik, “Emerging weak localization effects on a topological insulator–insulating ferromagnet ( $\text{Bi}_2\text{Se}_3$ -EuS) interface,” *Physical Review B* **88**, 081407(R) (2013).
- [17] Changmin Lee, Ferhat Katmis, Pablo Jarillo-Herrero, Jagadeesh S. Moodera, and Nuh Gedik, “Direct measurement of proximity-induced magnetism at the interface between a topological insulator and a ferromagnet,” *Nature Communications* **7** (2016), 10.1038/ncomms12014.
- [18] Chi Tang, Cui-Zu Chang, Gejian Zhao, Yawen Liu, Zilong Jiang, Chao-Xing Liu, Martha R. McCartney, David J. Smith, Tingyong Chen, Jagadeesh S. Moodera, and Jing Shi, “Above 400-k robust perpendicular ferromagnetic phase in a topological insulator,” *Science Advances* **3**, e1700307 (2017).
- [19] Shilei Zhang, Florian Kronast, Gerrit van der Laan, and Thorsten Hesjedal, “Real-space observation of skyrmionium in a ferromagnet-magnetic topological insulator heterostructure,” *Nano Letters* **18**, 1057–1063 (2018), pMID: 29363315, <https://doi.org/10.1021/acs.nanolett.7b04537>.
- [20] Naoto Nagaosa and Yoshinori Tokura, “Topological properties and dynamics of magnetic skyrmions,” *Nature Nanotechnology* **8**, 899–911 (2013).
- [21] Albert Fert, Nicolas Reyren, and Vincent Cros, “Magnetic skyrmions: advances in physics and potential applications,” *Nature Reviews Materials* **2**, 17031 (2017).
- [22] Roland Wiesendanger, “Nanoscale magnetic skyrmions in metallic films and multilayers: a new twist for spintronics,” *Nature Reviews Materials* **1**, 16044 (2016).
- [23] A. N. Bogdanov and D. A. Yablonskiĭ, “Thermodynamically stable “vortices” in magnetically ordered crystals. the mixed state of magnets,” *Zh. Eksp. Teor. Fiz.* **95**, 178–182 (1989).
- [24] In contrast to the weak contribution from the nonlocal energy of the volume magnetostatic charges, which for a thin film scales quadratically with the thickness, the considered “magnetic charging energy” is linear with the thickness and, therefore, it can not be neglected.
- [25] Dimitrios Andrikopoulos and Bart Sorée, “Skyrmion electrical detection with the use of three-dimensional topological insulators/ferromagnetic bilayers,” *Scientific Reports* **7**, 17871 (2017).
- [26] Chao-Xing Liu, Xiao-Liang Qi, HaiJun Zhang, Xi Dai, Zhong Fang, and Shou-Cheng Zhang, “Model hamiltonian for topological insulators,” *Phys. Rev. B* **82**, 045122 (2010).
- [27] See the supplemental materials.
- [28] Jeongwoo Kim, Kyoung-Whan Kim, Hui Wang, Jairo Sinova, and Ruqian Wu, “Understanding the giant enhancement of exchange interaction in  $\text{Bi}_2\text{Se}_3$ -EuS heterostructures,” *Physical Review Letters* **119**, 027201 (2017).
- [29] For EuS we would have  $\rho_s = S^2[J_1 + J_2/2]/a_0 \approx 0.29$  meV/nm, where  $S = 7/2$  is spin of the Eu atom,  $J_1/k_B = 0.228$  K and  $J_2/k_B = -0.118$  K are the nearest and next-nearest neighbor exchange energies, respectively, and for the lattice spacing  $a_0 = 5.968$  Å [50].
- [30] C. Moreau-Luchaire, C. Moutafis, N. Reyren, J. Sampaio, C. A. F. Vaz, N. Van Horne, K. Bouzehouane, K. Garcia, C. Deranlot, P. Warnicke, P. Wohlhuter, J.-M. George, M. Weigand, J. Raabe, V. Cros, and A. Fert, “Additive interfacial chiral interaction in multilayers for stabilization of small individual skyrmions at room temperature,” *Nature Nanotech* **11**, 444–448 (2016).
- [31] Anjan Soumyanarayanan, M. Raju, A. L. Gonzalez Oyarce, Anthony K. C. Tan, Mi-Young Im, A. P. Petrović, Pin Ho, K. H. Khoo, M. Tran, C. K. Gan, F. Ernult, and C. Panagopoulos, “Tunable room-temperature magnetic skyrmions in ir/fe/co/pt multilayers,” *Nature Materials* **16**, 898–904 (2017).
- [32] Olivier Boulle, Jan Vogel, Hongxin Yang, Stefania Pizzini, Dayane de Souza Chaves, Andrea Locatelli, Tevfik Onur Menteş, Alessandro Sala, Liliana D. Buda-Prejbeanu, Olivier Klein, Mohamed Belmeguenai, Yves Roussigné, Andrey Stashkevich, Salim Mourad Chérif, Lucia Aballe, Michael Foerster, Mairbek Chshiev, Stéphane Auffret, Ioan Mihai Miron, and Gilles Gaudin, “Room-temperature chiral magnetic skyrmions in ultrathin magnetic nanostructures,” *Nature Nanotech* (2016), 10.1038/nnano.2015.315.
- [33] Seonghoon Woo, Kai Litzius, Benjamin Kruger, Mi-Young Im, Lucas Caretta, Kornel Richter, Maxwell Mann, Andrea Krone, Robert M. Reeve, Markus Weigand, Parnika Agrawal, Ivan Lemesh, Mohamad-Assaad Mawass, Peter Fischer, Mathias Klaui, and Geoffrey S. D. Beach, “Observation of room-temperature magnetic skyrmions and their current-driven dynamics in ultrathin metallic ferromagnets,” *Nature Materials* **15**, 501–506 (2016).
- [34] A. Bogdanov and A. Hubert, “Thermodynamically stable magnetic vortex states in magnetic crystals,” *Journal of Magnetism and Magnetic Materials* **138**, 255–269 (1994).
- [35] A. Bogdanov and A. Hubert, “The properties of isolated magnetic vortices,” *physica status solidi (b)* **186**, 527–543 (1994).
- [36] A. Bogdanov and A. Hubert, “The stability of vortex-like structures in uniaxial ferromagnets,” *Journal of Magnetism and Magnetic Materials* **195**, 182–192 (1999).
- [37] M. N. Wilson, A. B. Butenko, A. N. Bogdanov, and T. L. Monchesky, “Chiral skyrmions in cubic helimagnet films: The role of uniaxial anisotropy,” *Phys. Rev. B* **89**, 094411 (2014).
- [38] Christoph Schütte and Markus Garst, “Magnon-skyrmion scattering in chiral magnets,” *Phys. Rev. B* **90**, 094423 (2014).
- [39] U. K. Röbler, A. N. Bogdanov, and C. Pfleiderer, “Spontaneous skyrmion ground states in magnetic metals,” *Nature* **442**, 797–801 (2006).
- [40] A O Leonov, T L Monchesky, N Romming, A Kubetzka, A N Bogdanov, and R Wiesendanger, “The properties of isolated chiral skyrmions in thin magnetic films,” *New J. Phys.* **18**, 065003 (2016).
- [41] Milton Abramowitz and Irene A. Stegun, *Handbook of mathematical functions with formulas, graphs, and mathematical tables*, ninth Dover printing, tenth GPO printing ed. (Dover, New York, 1972).
- [42] Volodymyr P. Kravchuk, Denis D. Sheka, Ulrich K. Röbler, Jeroen van den Brink, and Yuri Gaididei, “Spin eigenmodes of magnetic skyrmions and the problem of the effective skyrmion mass,” *Phys. Rev. B* **97**, 064403 (2018).
- [43] B. A. Ivanov, H. J. Schnitzer, F. G. Mertens, and G. M. Wysin, “Magnon modes and magnon-vortex scattering in two-dimensional easy-plane ferromagnets,” *Phys. Rev. B* **58**, 8464–8474 (1998).
- [44] D. D. Sheka, B. A. Ivanov, and F. G. Mertens, “Internal modes and magnon scattering on topological solitons in

two-dimensional easy-axis ferromagnets,” *Phys. Rev. B* **64**, 024432 (2001).

- [45] Denis D. Sheka, Ivan A. Yastremsky, Boris A. Ivanov, Gary M. Wysin, and Franz G. Mertens, “Amplitudes for magnon scattering by vortices in two-dimensional weakly easy-plane ferromagnets,” *Phys. Rev. B* **69**, 054429 (2004).
- [46] B. A. Ivanov and D. D. Sheka, “Local magnon modes and the dynamics of a small-radius two-dimensional magnetic soliton in an easy-axis ferromagnet,” *JETP Lett.* **82**, 436–440 (2005).
- [47] D. D. Sheka, C. Schuster, B. A. Ivanov, and F. G. Mertens, “Dynamics of topological solitons in two-dimensional ferromagnets,” *The European Physical Journal B - Condensed Matter* **50**, 393–402 (2006).
- [48] The stability analysis was performed for zero temperature. However, thermally induced magnons would only result in additional damping for bounded skyrmion modes.
- [49] The exact value is  $e_{\text{ex}} = [\pi^2 + \gamma_0 - \text{Ci}(2\pi) + \ln(2\pi)]/2$ , where  $\gamma_0$  is Euler constant and  $\text{Ci}(x)$  denotes the cosine integral function, see [34].
- [50] A. Mauger and C. Godart, “The magnetic, optical, and transport properties of representatives of a class of

magnetic semiconductors: The europium chalcogenides,” *Physics Reports* **141**, 51 – 176 (1986).

- [51] The case  $\epsilon = 0$  was analysed earlier in Ref. [34].

## Supplemental Information

### Effective free energy and induced DM term

Let us consider the following low energy Hamiltonian for the Dirac fermions on the surface of the TI,

$$H_{\text{Dirac}} = [\mathbf{d}(-i\hbar\nabla) - J_0\mathbf{n}(\mathbf{r})] \cdot \boldsymbol{\sigma}. \quad (\text{S1})$$

Quite generally, the non-interacting Green function for a spin-momentum locked system can be written,

$$\mathcal{G}_{\alpha\beta}(X) = G(X)\delta_{\alpha\beta} + \mathbf{F}(X) \cdot \boldsymbol{\sigma}_{\alpha\beta}, \quad (\text{S2})$$

where  $X = (\tau, \mathbf{r})$ , with  $\tau \in [0, \beta]$  being the imaginary time. Thus, expanding the free energy expression up to  $J_0^2$ , we obtain  $F_{\text{Dirac}} = F_{\text{Dirac}}(0) + \delta F_{\text{Dirac}}$ , where,

$$\delta F_{\text{Dirac}} = \frac{1}{2} \int_X \int_{X'} \mathcal{G}_{\alpha\beta}(X - X') \mathcal{G}_{\gamma\delta}(X' - X) [J_0\mathbf{n}(X) \cdot \boldsymbol{\sigma}_{\beta\gamma}] [J_0\mathbf{n}(X') \cdot \boldsymbol{\sigma}_{\delta\alpha}], \quad (\text{S3})$$

where we use the shorthand notation  $\int_X \equiv \int_0^\beta d\tau \int d^2r$ . Lengthy but straightforward calculations yield,

$$\begin{aligned} \delta F_{\text{Dirac}}^{\text{mag}} = & \frac{J_0^2}{2} \int_X \int_{X'} \{2[G(X - X')G(X' - X) - \mathbf{F}(X - X') \cdot \mathbf{F}(X' - X)]\mathbf{n}(X) \cdot \mathbf{n}(X') \\ & + 4\mathbf{F}(X - X') \cdot \mathbf{n}(X)\mathbf{F}(X' - X) \cdot \mathbf{n}(X') - 24iG(X - X')\mathbf{F}(X' - X) \cdot [\mathbf{n}(X) \times \mathbf{n}(X')]\}, \end{aligned} \quad (\text{S4})$$

where in writing the above equation we have made use of the property  $\mathbf{F}(\tau, -\mathbf{r}) = -\mathbf{F}(\tau, \mathbf{r})$ .

Observe that Eq. (S4) features also the general Dzyloshinsky-Moriya (DM) term, which arises in the third line of that equation. It can be re-cast in a more familiar form by specializing to the simple case,

$$G(\omega_n, \mathbf{k}) = \frac{i\omega_n + \mu}{(i\omega_n + \mu)^2 - \mathbf{d}^2(\mathbf{k})}, \quad (\text{S5})$$

$$\mathbf{F}(\omega_n, \mathbf{k}) = -\frac{\mathbf{d}(\mathbf{k})}{(i\omega_n + \mu)^2 - \mathbf{d}^2(\mathbf{k})}, \quad (\text{S6})$$

where  $\omega_n = (2n + 1)\pi/\beta$  and  $\mathbf{d}(\mathbf{k})$  is either  $\mathbf{d}_1$  or  $\mathbf{d}_2$  from Eq. (2) in momentum space. Assuming a time-independent magnetization, Eq. (S4) becomes,

$$\delta F_{\text{Dirac}}^{\text{mag}} = \frac{J_0^2}{2} \int \frac{d^2k}{(2\pi)^2} [S_{ab}(\mathbf{k}) + A_c(\mathbf{k})\epsilon_{abc}] n_a(\mathbf{k}) n_b(-\mathbf{k}), \quad (\text{S7})$$

featuring symmetric and antisymmetric contributions  $S_{ab}$  and  $A_c$ , which are given by,

$$S_{ab}(\mathbf{k}) = \frac{2}{\beta} \sum_{n=-\infty}^{\infty} \int \frac{d^2q}{(2\pi)^2} \frac{[(i\omega_n + \mu)^2 - \mathbf{d}(\mathbf{q}) \cdot \mathbf{d}(\mathbf{q} + \mathbf{k})]\delta_{ab} + 2d_a(\mathbf{q})d_b(\mathbf{q} + \mathbf{k})}{[(i\omega_n + \mu)^2 - (\hbar v_F)^2 q^2][(i\omega_n + \mu)^2 - (\hbar v_F)^2 (\mathbf{q} + \mathbf{k})^2]}, \quad (\text{S8})$$

$$A_c(\mathbf{k}) = \frac{24i}{\beta} \sum_{n=-\infty}^{\infty} \int \frac{d^2q}{(2\pi)^2} \frac{(i\omega_n + \mu)d_c(\mathbf{q})}{[(i\omega_n + \mu)^2 - (\hbar v_F)^2 q^2][(i\omega_n + \mu)^2 - (\hbar v_F)^2 (\mathbf{q} + \mathbf{k})^2]}, \quad (\text{S9})$$

respectively.

The symmetric contribution induces a magnetization

stiffness at the interface. Part of the integral yielding  $S_{ab}$  does not converge and needs to be regularized by means of a cutoff  $\Lambda$ . The result in the long wavelength limit is,

$$S_{ab}(\mathbf{k}) = -\frac{\Lambda}{4\pi\hbar v_F} \delta_{ab} + \mathcal{S}(\beta, \mu) k^2 \left( \delta_{ab} + \frac{k_a k_b}{k^2} \right), \quad (\text{S10})$$

where  $\mathcal{S}(\beta, \mu) = \beta/[24\pi \cosh^2(\beta\mu/2)]$ .

The antisymmetric contribution vanishes for  $\mu = 0$ , since the Matsubara sum involves an odd summand in this case. Thus, in order to generate a DM term the chemical potential must be nonzero. Assuming  $\mu \neq 0$ , and a long wavelength limit, we obtain,

$$A_c(\mathbf{k}) = -id_c(\mathbf{k})\mathcal{A}(\beta\mu), \quad (\text{S11})$$

where  $\mathcal{A}(\beta\mu) = (8\pi\hbar v_F)^{-1} \tanh(\beta\mu/2)$ . Writing,

$$F_{\text{Dirac}}^{\text{mag}} = \int d^2r \mathcal{F}_{\text{Dirac}}^{\text{mag}}(\mathbf{n}(\mathbf{r})), \quad (\text{S12})$$

we obtain for the fluctuation correction of the free energy density,

$$\delta\mathcal{F}_{\text{Dirac}}^{\text{mag}} = \frac{s}{2} \{ [\nabla\mathbf{n}(\mathbf{r})]^2 + [\nabla \cdot \mathbf{n}(\mathbf{r})]^2 \} + i\frac{a}{2} \mathbf{n}(\mathbf{r}) \cdot [\mathbf{d}(-i\hbar\nabla) \times \mathbf{n}(\mathbf{r})], \quad (\text{S13})$$

where  $(\nabla\mathbf{n})^2 = \sum_{i=x,y,z} (\nabla n_i)^2$  defines the usual exchange term, and we have defined  $s = J_0^2 \mathcal{S}(\beta, \mu)$  and  $a = J_0^2 \mathcal{A}(\beta, \mu)$ . A term proportional to  $\Lambda \mathbf{n}^2$  implied by the first term in (S10) has been removed, since it is actually a constant in view of the constraint  $\mathbf{n}^2 = 1$ . Similarly, we can drop the constant term  $F_{\text{Dirac}}(0)$  from the free energy, since it does not depend on the field. Thus, we can safely write  $\mathcal{F}_{\text{Dirac}} = \delta\mathcal{F}_{\text{Dirac}}$ . The above expression features a DM term induced by Dirac fermion fluctuations. In addition, a contribution  $\sim (\nabla \cdot \mathbf{n})^2$  is also generated. This term leads to interesting physical properties when  $\mathbf{d}_2$  is replaced for  $\mathbf{d}$  in Eq. (S13), modifying in this way the behavior of Néel skyrmions. Note that differently from the case where the Dirac fermion is gapped [15], no intrinsic anisotropy is generated by the Dirac fermions.

### One-dimensional magnetization modulation

Here we consider one-dimensional static solutions  $\mathbf{n} = \mathbf{n}(x)$  of the model (8). Let us start with the case  $\mathcal{E}_{\text{DMI}} = \mathcal{E}_{\text{DMI}}^{\text{N}}$ . In this case the effective energy  $E_{\text{eff}} = AL \int \mathcal{E}_{\text{1D}}^{\text{N}} d^2x$  is described by the density

$$\mathcal{E}_{\text{1D}}^{\text{N}} = \theta'^2 + \sin^2 \theta \phi'^2 + \epsilon (\cos \theta \cos \phi \theta' - \sin \theta \sin \phi \phi')^2 + d (\cos \phi \theta' - \sin \theta \cos \theta \sin \phi \phi') + 2(1 - \cos \theta), \quad (\text{S14})$$

where angles  $\theta(x)$  and  $\phi(x)$  determine orientation of the unit magnetization vector  $\mathbf{n} = \sin \theta (\cos \phi \hat{\mathbf{x}} + \sin \phi \hat{\mathbf{y}}) +$

$\cos \theta \hat{\mathbf{z}}$ , prime denotes the derivation with respect to the dimensionless coordinate  $x$  measured in units of  $\ell$ . The corresponding Euler-Lagrange equations  $\delta E_{\text{eff}}/\delta \theta = 0$  and  $\delta E_{\text{eff}}/\delta \phi = 0$  are as follows

$$\theta'' - \sin \theta \cos \theta \phi'^2 - \epsilon \cos \theta \cos \phi \Xi \quad (\text{S15a})$$

$$- d \sin^2 \theta \sin \phi \phi' - \sin \theta = 0,$$

$$(\sin^2 \theta \phi')' + \epsilon \sin \theta \sin \phi \Xi + d \sin^2 \theta \sin \phi \theta' = 0, \quad (\text{S15b})$$

where

$$\Xi = \cos \theta [2 \sin \phi \theta' \phi' - \cos \phi \theta''] + \sin \theta [\cos \phi (\theta'^2 + \phi'^2) + \sin \phi \phi'']. \quad (\text{S15c})$$

First of all, Eqs. (S15) have trivial solution  $\theta = 0$ , which corresponds to the uniform magnetization along the field  $\mathbf{n} = \hat{\mathbf{z}}$ . The uniform state has zero energy  $\mathcal{E}_{\text{1D}}^{\text{N}} = 0$ . The another trivial solution  $\theta = \pi$  ( $\mathbf{n} = -\hat{\mathbf{z}}$ ) corresponds to the energy maximum and it is unstable.

Let us consider possible nonuniform solutions. Equation (S15b) is satisfied when  $\sin \phi = 0$  ( $\phi = 0$  for  $d\theta' < 0$ , and  $\phi = \pi$  for  $d\theta' > 0$ ), or in the other words  $n_y = 0$ . Thus, the magnetization lies within the plane  $\hat{\mathbf{x}}\theta\hat{\mathbf{z}}$ . The components  $n_x = \sin \theta$  and  $n_z = \cos \theta$  are determined by the equation (S15a), which now looks has a form

$$\theta'' (1 + \epsilon \cos^2 \theta) = \sin \theta (1 + \epsilon \cos \theta \theta'^2), \quad (\text{S16})$$

and the corresponding energy density reads

$$\mathcal{E} = \theta'^2 (1 + \epsilon \cos^2 \theta) + 4 \sin^2 \frac{\theta}{2} - d\theta', \quad (\text{S17})$$

where we assumed that  $d\theta' > 0$ . Rewriting the Eq. (S16) in form  $[\theta'^2 (1 + \epsilon \cos^2 \theta)]' = -2(\cos \theta)'$  one can easily find its first integral

$$\theta'^2 (1 + \epsilon \cos^2 \theta) = 4 \sin^2 \frac{\theta}{2} + 4C, \quad (\text{S18})$$

where  $C$  is the integration constant. Equation (S18) admits separation of the variables and can be solved in quadratures. The constant  $C$  determines period  $T$  of the magnetization structure:  $\mathbf{n}(x+T) = \mathbf{n}(x)$ . Let us first consider the particular case  $C = 0$ , it corresponds to a solution of (S18), which satisfies the boundary conditions  $\theta(-\infty) = 0$ ,  $\theta(+\infty) = 2\pi$  (or vice-versa), this is a single  $2\pi$ -domain wall of Néel type, in this case  $T \rightarrow \infty$ . Taking into account (S18) and (S17) one can present energy  $E_{\text{DW}} = \int_{-\infty}^{+\infty} \mathcal{E} dx$  of this domain wall in form

$$E_{\text{DW}} = 8 \int_0^\pi \sin \theta \sqrt{1 + \epsilon \cos^2 \theta} d\theta - 2\pi d. \quad (\text{S19})$$

The condition  $E_{\text{DW}} < 0$ , or equivalently

$$d > d_c^{\text{N}}(\epsilon) = \frac{8}{\pi} \int_0^1 \sqrt{1 + \epsilon(2\xi^2 - 1)^2} d\xi, \quad (\text{S20})$$



determines the area of parameters, where nucleation of the  $2\pi$ -domain wall on the background of the saturated state  $\mathbf{n} = \hat{z}$  is energetically preferable.

The general case  $C > 0$  corresponds to the helical state, which can be interpreted as a periodical sequence of the considered domain walls. If  $\epsilon = 0$  [51], then the solution of (S18) reads

$$\theta = 2 \operatorname{am} \left( \sqrt{C}(x - x_0) \middle| -\frac{1}{C} \right), \quad (\text{S21})$$

where  $\operatorname{am}(x|k)$  is Jacobi's amplitude function [41] and the integration constant  $x_0$  determines a uniform shift along  $x$ -axis. The solution (S21) determines period of the magnetization components  $n_x = \sin \theta$  and  $n_z = \cos \theta$ :

$$T = \frac{2}{\sqrt{C}} K \left( -\frac{1}{C} \right), \quad (\text{S22})$$

where  $K(k)$  is complete elliptic integral of the first kind [41]. The constant  $C$  must be found from the minimization of the total energy per period  $E_T^N = T^{-1} \int_0^T \mathcal{E} dx$ . Performing the minimization procedure for (S21) and (S22) one obtains  $E_T^N = -4C$  for energy of the equilibrium structure, where the equilibrium value of the constant  $C$  is determined by the equation

$$\frac{d}{d_c^N(0)} = \sqrt{C} E \left( -\frac{1}{C} \right) \quad (\text{S23})$$

with  $E(k)$  being the complete elliptic integral of the second kind. The total energy (8) per period reads  $E_{1D}^N = ALE_T^N$ . An example of a solution for the case  $\epsilon = 0$  is shown in Fig. S1(a) by the black line.

For the case  $\epsilon > 0$ , the solution of Eq. (S18), which minimizes the energy  $E_T^N(C)$  with respect to  $C$  can be found only numerically. An example for the case  $\epsilon = 1$  is shown in Fig. S1(a) by the red solid line. As one can see, the  $\epsilon$ -term can noticeably increase period of the structure. It is important to note that one can avoid the tedious procedure of the numerical minimization of the energy  $E_T^N(C)$  by using the fact that the equilibrium value  $C \approx \tilde{C}$ , where  $\tilde{C}$  is found in the way analogous to (S23):

$$\frac{d}{d_c(\epsilon)} = \sqrt{\tilde{C}} E \left( -\frac{1}{\tilde{C}} \right). \quad (\text{S24})$$

An example of such an approximate solution is shown in Fig. S1(a) by the red dashed line. And the corresponding energy per period can be well approximated as  $E_T^N \approx -4\tilde{C}$ , see Fig. S1(b).

Let us now proceed to the case  $\mathcal{E}_{\text{DMI}} = \mathcal{E}_{\text{DMI}}^B$ . In this case the energy density coincides with (S14) but the DMI-term

$$\begin{aligned} \mathcal{E}_{1D}^B = & \theta'^2 + \sin^2 \theta \phi'^2 + \epsilon (\cos \theta \cos \phi \theta' - \sin \theta \sin \phi \phi')^2 \\ & + d (\sin \phi \theta' + \sin \theta \cos \theta \cos \phi \phi') + 2(1 - \cos \theta). \end{aligned} \quad (\text{S25})$$

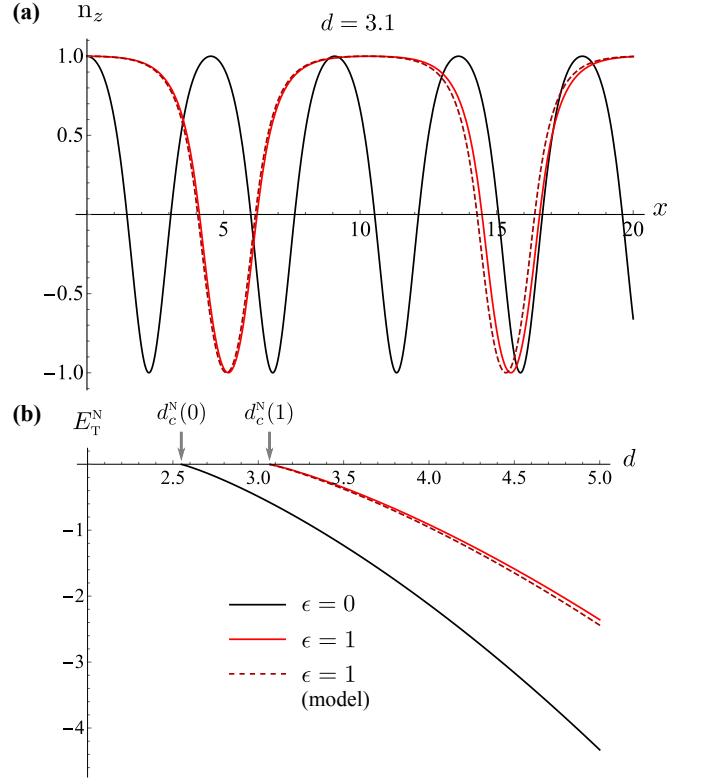


FIG. S1. Influence of the  $\epsilon$ -term on 1D periodical structure. (a) – perpendicular magnetization component  $n_z$ ; (b) – energy per period. The dashed line corresponds to the approximations: (a) the solution of Eq. (S18) with  $C = \tilde{C}$ , where  $\tilde{C}$  is determined by (S24); (b)  $\tilde{E}_T^N = -4\tilde{C}$ .

Energy expression (S25) generates the Euler-Lagrange equations

$$\theta'' - \sin \theta \cos \theta \phi'^2 - \epsilon \cos \theta \cos \phi \Xi \quad (\text{S26a})$$

$$+ d \sin^2 \theta \cos \phi \phi' - \sin \theta = 0,$$

$$(\sin^2 \theta \phi')' + \epsilon \sin \theta \sin \phi \Xi - d \sin^2 \theta \cos \phi \theta' = 0, \quad (\text{S26b})$$

which coincide with (S15) up to the replacement  $\sin \phi \leftrightarrow -\cos \phi$  in the DMI terms. As a result, equation (S26b) is satisfied when  $\cos \phi = 0$  (in this case  $\Xi = 0$ ), or in the other words  $n_x = 0$ . Thus, the magnetization lies within the plane  $\hat{y}\hat{0}\hat{z}$ . The latter corresponds to the Bloch domain walls. The components  $n_y = \sin \theta$  and  $n_z = \cos \theta$  are determined by the equation (S26a), which coincides with (S16) if  $\epsilon = 0$ . Thus,  $\epsilon$  does not effect the static 1D solution for the case  $\mathcal{E}_{\text{DMI}} = \mathcal{E}_{\text{DMI}}^B$  and the further analysis coincides with the one done for  $\mathcal{E}_{\text{DMI}} = \mathcal{E}_{\text{DMI}}^N$  with  $\epsilon = 0$ .

### Skyrmion solutions

Let us consider two-dimensional solutions. As previously, we first consider the case  $\mathcal{E}_{\text{DMI}} = \mathcal{E}_{\text{DMI}}^N$ . Introducing the normalized in-plane magnetization component

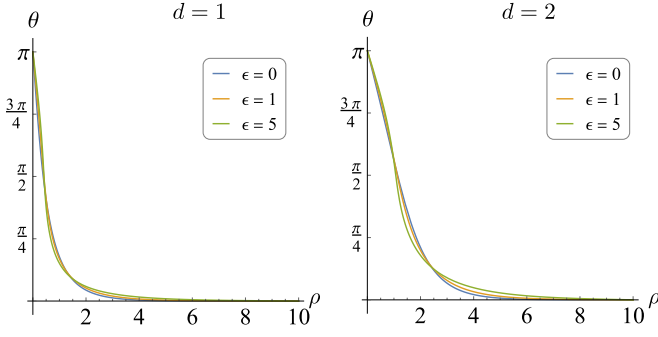


FIG. S2. Skymion profiles determined by Eq. (9) for various values of parameters  $d$  and  $\epsilon$ .

$\boldsymbol{\eta} = \cos \phi \hat{\boldsymbol{x}} + \sin \phi \hat{\boldsymbol{y}}$  one can present the energy density in the form

$$\begin{aligned} \mathcal{E}_{2D}^N = & (\nabla \theta)^2 + \sin^2 \theta (\nabla \phi)^2 + \epsilon [\nabla \cdot (\sin \theta \boldsymbol{\eta})]^2 \\ & + 2d \sin^2 \theta (\boldsymbol{\eta} \cdot \nabla \theta) + 4 \sin^2 \frac{\theta}{2}. \end{aligned} \quad (\text{S27})$$

The corresponding Euler-Lagrange equations  $\delta E_{\text{eff}}/\delta \theta = 0$  and  $\delta E_{\text{eff}}/\delta \phi = 0$  read

$$\nabla^2 \theta + \epsilon \cos^2 \theta \nabla \cdot [\boldsymbol{\eta} (\nabla \theta \cdot \boldsymbol{\eta})] \quad (\text{S28a})$$

$$- \sin \theta \cos \theta \{ (\nabla \phi)^2 + \epsilon [(\nabla \theta \cdot \boldsymbol{\eta})^2 - \boldsymbol{\eta} \cdot \nabla (\nabla \cdot \boldsymbol{\eta})] \} \\ + d \sin^2 \theta \nabla \cdot \boldsymbol{\eta} - \sin \theta = 0,$$

$$\nabla \cdot [\sin^2 \theta \nabla \phi] - d \sin^2 \theta (\bar{\boldsymbol{\eta}} \cdot \nabla \theta) \quad (\text{S28b})$$

$$+ \epsilon \sin^2 \theta [\bar{\boldsymbol{\eta}} \cdot \nabla (\nabla \cdot \boldsymbol{\eta}) - (\nabla \theta \cdot \boldsymbol{\eta})(\nabla \theta \cdot \bar{\boldsymbol{\eta}})] \\ + \epsilon \sin \theta \cos \theta [(\nabla \theta \cdot \bar{\boldsymbol{\eta}}) \nabla \cdot \boldsymbol{\eta} + \bar{\boldsymbol{\eta}} \cdot \nabla (\nabla \theta \cdot \boldsymbol{\eta})] = 0,$$

where  $\bar{\boldsymbol{\eta}} = \partial_\phi \boldsymbol{\eta} = -\sin \phi \hat{\boldsymbol{x}} + \cos \phi \hat{\boldsymbol{y}}$  is the unit vector perpendicular to  $\boldsymbol{\eta}$ . Equations (S28) have trivial solution  $\theta = 0$ . Besides, the Eq. (S28b) is always satisfied if  $\boldsymbol{\eta} = \mathbf{const}$  and  $\theta = \theta(\xi)$  with  $\xi$  being a coordinate along  $\boldsymbol{\eta}$ . This is the one-dimensional case considered in the previous section. The analogous ‘‘one-dimensional’’ solution takes place in the curvilinear polar frame of reference  $\{\rho, \chi\}$ . Indeed, in this case the Eq. (S28b) is satisfied if  $\boldsymbol{\eta} = \mathbf{e}_\rho$  (equivalently  $\phi = \chi$ ) and  $\theta = \theta(\rho)$ . Here-with, Eq. (S28a) is reduced to Eq. (9), which describes profile of the isolated skymion. Note that for the case  $d < 0$  the in-plane magnetization is  $\boldsymbol{\eta} = -\mathbf{e}_\rho$  (equivalently  $\phi = \chi + \pi$ ). Few examples of skymion profiles determined by Eq. (9) for various values of parameters  $d$  and  $\epsilon$  are shown in Fig. S2. Note that the skymion size is mainly determined by the parameter  $d$ , while the parameter  $\epsilon$  weakly modifies details of the skymion profile.

Let us now consider stability of the static skymion solutions of Eq. (9). To this end we introduce small deviations  $\theta = \theta_0 + \vartheta$  and  $\phi = \phi_0 + \varphi/\sin \theta_0$  of the static profile  $\theta_0 = \theta_0(\rho)$ ,  $\phi_0 = \chi$ . Landau-Lifshitz equations  $\sin \theta \partial_t \phi = \frac{\gamma}{M_s} \delta E_{\text{eff}}/\delta \theta$ ,  $-\sin \theta \partial_t \theta = \frac{\gamma}{M_s} \delta E_{\text{eff}}/\delta \phi$

linearized in vicinity of the static solution with respect to the deviations  $\vartheta$  and  $\varphi$  are as follows

$$\begin{aligned} \dot{\varphi} &= \hat{H}_1 \vartheta + W_1 \partial_\chi \varphi + V \partial_{\rho\chi}^2 \varphi, \\ -\dot{\vartheta} &= \hat{H}_2 \varphi - W_2 \partial_\chi \vartheta + V \partial_{\rho\chi}^2 \vartheta, \end{aligned} \quad (\text{S29})$$

where dot indicates the derivative with respect to the dimensionless time  $\tau = t\Omega_0$  with  $\Omega_0 = \gamma H$  being the Larmor frequency. The differential operators and the potentials read

$$\begin{aligned} \hat{H}_1 &= -\nabla_\rho^2 - \frac{\epsilon}{\rho} \partial_\rho (\rho \cos^2 \theta_0 \partial_\rho) - \frac{1}{\rho^2} \partial_{\chi\chi}^2 + U_1, \\ \hat{H}_2 &= -\nabla_\rho^2 - \frac{1+\epsilon}{\rho^2} \partial_{\chi\chi}^2 + U_2, \\ U_1 &= \cos 2\theta_0 \left( \frac{1+\epsilon}{\rho^2} + \epsilon \theta_0'^2 \right) + \epsilon \sin 2\theta_0 \nabla_\rho^2 \theta_0 \\ &\quad - \frac{d}{\rho} \sin 2\theta_0 + \cos \theta_0, \\ U_2 &= (1+\epsilon) (\cot \theta_0 \nabla_\rho^2 \theta_0 - \theta_0'^2) - \frac{\epsilon}{\rho^2} - d\theta_0', \\ W_1 &= \frac{2+\epsilon}{\rho^2} \cos \theta_0 - \frac{d}{\rho} \sin \theta_0, \\ W_2 &= W_1 - \frac{\epsilon}{\rho} \sin \theta_0 \theta_0', \quad V = -\frac{\epsilon}{\rho} \cos \theta_0. \end{aligned} \quad (\text{S30})$$

Note that term  $(\nabla \cdot \mathbf{n})^2$  leads to the mixing of the derivatives in the linearized equations (S29) (the  $V$ -term). This is in contrast to the corresponding linear equations previously obtained for magnons over precessional solitons in easy-axis magnets [44, 46, 47], magnetic vortices in easy-plane magnets [43, 45], and magnetic skymions [38, 42].

Equations (S29) have solution  $\vartheta = f(\rho) \cos(\omega\tau + \mu\chi + \chi_0)$ ,  $\varphi = g(\rho) \sin(\omega\tau + \mu\chi + \chi_0)$ , where  $\mu \in \mathbb{Z}$  is azimuthal quantum number and  $\chi_0$  is an arbitrary phase. The eigenfrequencies  $\omega$  and the corresponding eigenfunctions  $f, g$  are determined by the following generalized eigen-value problem (EVP)

$$\hat{\mathcal{H}} \boldsymbol{\psi} = \omega \hat{\sigma}_x \boldsymbol{\psi}, \quad \hat{\mathcal{H}} = \left\| \begin{array}{cc} \hat{\mathcal{H}}_1 & \mu(W_1 + V \partial_\rho) \\ \mu(W_2 - V \partial_\rho) & \hat{\mathcal{H}}_2 \end{array} \right\| \quad (\text{S31})$$

where  $\boldsymbol{\psi} = (f, g)^T$  and  $\hat{\sigma}_x$  is the first Pauli matrix. The diagonal operators are as follows

$$\begin{aligned} \hat{\mathcal{H}}_1 &= -\nabla_\rho^2 - \frac{\epsilon}{\rho} \partial_\rho (\rho \cos^2 \theta_0 \partial_\rho) + \frac{\mu^2}{\rho^2} + U_1 \\ \hat{\mathcal{H}}_2 &= -\nabla_\rho^2 + \frac{(1+\epsilon)\mu^2}{\rho^2} + U_2. \end{aligned} \quad (\text{S32})$$

EVP (S31) was solved numerically for a range of  $d$  and a couple of values of  $\epsilon$ , see Fig. 1(a) and discussion in the main text.

For the case  $\mathcal{E}_{\text{DMI}} = \mathcal{E}_{\text{DMI}}^B$  the energy expression coincides with (S27), but the DMI term

$$\begin{aligned} \mathcal{E}_{2D}^B = & (\nabla \theta)^2 + \sin^2 \theta (\nabla \phi)^2 + \epsilon [\nabla \cdot (\sin \theta \boldsymbol{\eta})]^2 \\ & + 2d \sin^2 \theta [\nabla \theta \times \boldsymbol{\eta}]_z + 4 \sin^2 \frac{\theta}{2}. \end{aligned} \quad (\text{S33})$$

The corresponding Euler-Lagrange equations coincide with (S28), where the replacement  $\boldsymbol{\eta} \leftrightarrow \bar{\boldsymbol{\eta}}$  is made in the DMI term (and only in this term). The second equation is satisfied if  $\boldsymbol{\eta} = \mathbf{e}_x$ , this corresponds to a Bloch skyrmion. The skyrmion profile is determined by the first equation, which in this case coincides with Eq. (9) with  $\epsilon = 0$ . Thus,  $\epsilon$  has no influence on static profiles of the Bloch skyrmion.

The corresponding linearized Landau-Lifshitz equations coincide with (S29) but the form of the differential operators and potentials

$$\begin{aligned}
\hat{H}_1 &= -\nabla_\rho^2 - \frac{1 + \epsilon \cos^2 \theta_0}{\rho^2} \partial_{xx}^2 + U_1, \\
\hat{H}_2 &= -(1 + \epsilon) \nabla_\rho^2 - \frac{1}{\rho^2} \partial_{xx}^2 + U_2, \\
U_1 &= \frac{\cos 2\theta_0}{\rho^2} - d \frac{\sin 2\theta_0}{\rho} + \cos \theta_0, \\
U_2 &= \cot \theta_0 \nabla_\rho^2 \theta_0 - \theta_0'^2 + \frac{\epsilon}{\rho^2} - d\theta_0', \\
W_1 &= \frac{2 + \epsilon}{\rho^2} \cos \theta_0 - \frac{d}{\rho} \sin \theta_0, \\
W_2 &= W_1 + \frac{\epsilon}{\rho} \sin \theta_0 \theta_0', \quad V = \frac{\epsilon}{\rho} \cos \theta_0.
\end{aligned} \tag{S34}$$

As for the previous case, the solution of the linear problem is reduced to a generalized EVP, which coincides with (S31) but the potentials are determined by (S34) and the diagonal operators are as follows

$$\begin{aligned}
\hat{\mathcal{H}}_1 &= -\nabla_\rho^2 + \frac{\mu^2(1 + \epsilon \cos^2 \theta_0)}{\rho^2} + U_1 \\
\hat{\mathcal{H}}_2 &= -(1 + \epsilon) \nabla_\rho^2 + \frac{\mu^2}{\rho^2} + U_2.
\end{aligned} \tag{S35}$$

The corresponding EVP (S31) was solved numerically for a range of  $d$  and a couple of values of  $\epsilon$ , see Fig. 1(b) and discussion in the main text.